International Journal of Refractory Metals & Hard Materials 87 (2020) 105135

Contents lists available at ScienceDirect

International Journal of Refractory Metals & Hard Materials

journal homepage: www.elsevier.com/locate/IJRMHM

The effect of hot isostatic pressing on thermal conductivity of additively manufactured pure tungsten

Jinhan Chen[a], Kailun Li[a], Yafei Wang[a], Leilei Xing[a], Chenfan Yu[a], Hailong Liu[a], Jing Ma[a], Wei Liu[a,*], Zhijian Shen[a,b,*]

[a] State Ley Laboratory of New Ceramic and Fine Processing, School of Materials Science and Engineering, Tsinghua University, Beijing 100084, China
[b] Department of Materials and Environmental Chemistry, Arrhenius Laboratory, Stockholm University, S-106 91 Stockholm, Sweden

ARTICLE INFO

Keywords:
Additive manufacturing
Thermal conductivity
Tungsten
Hot isostatic pressing
Microstructure

ABSTRACT

The crack-healing behaviors and microstructure evolution of pure tungsten produced by laser powder bed fusion (LPBF) were studied and compared before and after post hot isostatic pressing (post-HIP) treatment. An average thermal conductivity of 133 $W{\cdot}m^{-1}{\cdot}K^{-1}$ at room temperature (RT) was obtained after HIP, which was 16% higher than that of as-built sample (115 $W{\cdot}m^{-1}{\cdot}K^{-1}$). Although the HIP process had little effect on density, it resulted in a large grain size of > 300 μm accompanied by a decrease in dislocation density and crack healing, which led to a substantial improvement of thermal conductivity of pure tungsten. The positive correlation between relative density and thermal conductivity of as-built tungsten was reported.

1. Introduction

Due to its high melting point, high strength, good thermal conductivity and oxidation resistance, tungsten has been widely used in the electronic and medical industries. It has also been considered as a potential candidate for plasma-facing materials (PFMs) for divertors in future nuclear fusion devices in view of its excellent radiation-shielding properties against heat and plasma flux. When used as a plasma-facing component (PFC), the divertor would be exposed to steady state heat loads over 20 MW/m^2, which requires a complex structure to survive the severe environment [1–4]. At present, tungsten parts in industrial scale are commonly produced by powder metallurgy (PM). However, the intrinsic characteristics of high brittleness and hardness of tungsten make PM tungsten parts very difficult to be machined into complex shapes. Additive manufacturing (AM) is gaining popularity for manufacturing complex net shaped parts of many materials, therefore bringing about the possibility to overcome the shortcomings mentioned above [5,6]. As a relatively new manufacturing technology, one of the AM family members, laser powder bed fusion (LPBF), is increasingly emerging as an alternative to conventional methods, such as forging and casting, to lower the cost of production of components with complex geometries [7].

Removal of high heat flux is considered as one of the main functions of the divertor in a fusion reactor [4], which is strongly determined by the thermal property of tungsten that in turn can be influenced by the presence of large voids and cracks, as well as defects such as dislocations and grain boundaries [8]. Therefore, it is desirable to eliminate macro and micro defects in order to improve the thermal conductivity of AM tungsten to reach ITER grade [9,10]. It remains, however, a great challenge to make dense and crack-free tungsten parts because the high cohesive energy and high surface tension of molten tungsten reduce the melt pool flowability.

Although tungsten parts with over 97% of the theoretical density (TD) have been additively manufactured by using fine spherical powders and appropriate laser power [11,12], it was noticed that the large residual stress caused by high temperature gradients and rapid solidification during LPBF process may exceed the fracture strength of tungsten, leading to severe cracking. Modifying LPBF processing parameters may reduce cracking [13]. Preheating of the substrate is another way to reduce thermal stress thus to prevent cracking during LPBF. However, the required high preheating temperatures ($> 0.5 \times T_{melting}$) often result in the formation of satellite powders adjoined to the scan tracks, where the balling effect may offset the positive effect of deeper remelting and generate defects subsequently [14,15]. Nearly dense bulk components with fewer micro-cracks have been fabricated by solid-solution strengthened alloys and particle dispersion strengthened tungsten alloys [16,17]. The major drawback of the latter two methods is the lower thermal conductivity of the formed alloy samples compared

* Corresponding authors at: State Ley Laboratory of New Ceramic and Fine Processing, School of Materials Science and Engineering, Tsinghua University, Beijing 100084, China.
E-mail addresses: liuw@mail.tsinghua.edu.cn (W. Liu), shen@mmk.su.se (Z. Shen).

https://doi.org/10.1016/j.ijrmhm.2019.105135
Received 9 September 2019; Received in revised form 30 September 2019; Accepted 16 October 2019
Available online 06 November 2019

with the ITER grade tungsten (162 $W \cdot m^{-1} \cdot K^{-1}$ at RT [18]) as a consequence of the increased lattice distortion caused by atomic coherence and solid-solution. Accordingly, an effective way of enhancing the intrinsic thermal conductivity of additive manufactured pure tungsten remains to be found.

Hot isostatic pressing (HIP), as a pressure assisted densification process, has been widely used in post-treatment for casting materials and additive manufactured metallic components to eliminate defects such as cavities, voids and hot cracks [19–21]. It can also homogenize microstructures and reduce cracks without distorting the macro shape of as-built components. A favorable thermal conductivity of sintered tungsten alloys has been revealed by an integrated heat treatment in HIP at different temperatures [22]. However, how HIP treatment affects the thermal conductivity of additive manufactured pure metals due to the microstructure evolution has not been studied. This study aims to assess and understand the effect of HIP on the microstructural and micro-cracking behaviors. Thermal conductivities of as-built tungsten were correlated to the processing parameters, achieved relative density and microstructures. The mechanism of improving thermal conductivity of LPBFed W using post-HIP treatment was also discussed.

2. Experimental procedures

2.1. Powders and LPBF process

Spherical tungsten powders (purity > 99.9%, average particle size of 32 μm) suitable for LPBF process were used in this study. The powders were spheroidized using a plasma spheroidization machine (TekSphero-40, Tekna Co. Ltd., Sherbrooke, QC, Canada). The morphology of the spheroidized tungsten powder is shown in Fig. 1.

The LPBF experiments were carried out at a SLM 125HL machine (SLM-Solutions Group AG, Germany) using a 400 W Yb/YAG fiber continual wave laser with a laser beam diameter of 80 μm. Cuboidal samples of dimensions 10 mm × 10 mm × 2 mm with 1 mm high supports were fabricated on tungsten substrates using different process parameters: laser power (P = 400 W), scanning speed (v = 100–700 mm/s), layer thickness (t = 30 μm), hatch distance (h = 100–120 μm). 100 μm hatch distance was selected as an optimized parameter for HIP processing subsequently. To limit the oxidation of tungsten, the fabrication process was carried out under a high-purity argon environment to maintain the oxygen content below 500 ppm. A zig-zag scanning strategy was utilized with an intra-layer rotation of 67°, which is beneficial to minimize the residual thermal stresses.

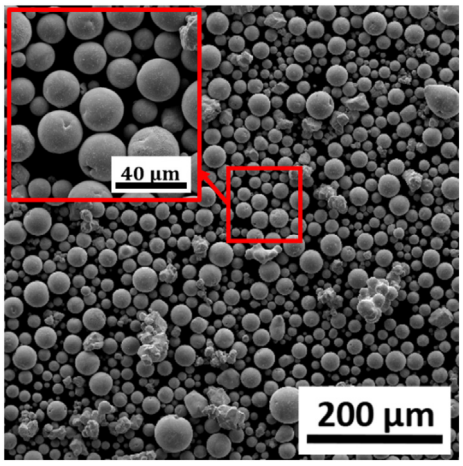

Fig. 1. Characteristic morphologies of spheroidized pure tungsten powder revealed by an SEM image.

2.2. Post-LPBF procedures and materials characterization

Post-LPBF treatment (1800 °C, 4 h/ 180 MPa) was carried out in a HIP facility (QIH-15, Quintus Technologies, Sweden), with a maximum operating temperature of 2000 °C and a maximum pressure of 200 MPa in a pure Ar atmosphere. Thermal diffusivity (α) was measured by a laser flash diffusivity system (LFA457 Micro flash, NETZSCH, Germany) at RT. Each as-built and HIPed sample was measured three times along the building direction (BD) to obtain a mean thermal diffusivity. The thermal conductivity (γ) was calculated according to the equation:

$$\gamma = \alpha C_p \rho \quad (1)$$

where α is the thermal diffusivity, ρ is the relative density, and C_p is the specific heat. The specific heat data was acquired from Ref. [23]. The density of samples was measured by Archimedes' method.

The samples were mechanically ground using conventional metallographic methods followed by electropolishing in a 1.5 wt% NaOH solution at a voltage of 9.8 V for 90 s. Top and side view cross-sections were characterized using a TESCAN MIRA 3LMH scanning electron microscope (SEM, TESCAN, Bron, Czech Republic). The microstructure and local crystallographic orientation were acquired using an electron backscatter diffraction (EBSD) detector on an HKL Nordlys orientation imaging microscope system (Oxford Instruments, Oxford, UK). The misorientation data obtained from the EBSD scan was analyzed using HKL Channel 5 software packages.

3. Results and discussions

3.1. Density and thermal conductivity of as-built and post-HIPed tungsten samples

Fig. 2 shows the variations of thermal conductivity and relative density of as-built samples with different hatch distance and scanning speed. It appears that no samples were fully dense; their relative density is in the range of 90% to 97%. A maximum thermal conductivity of 129 W/ (m· K) was observed in a sample with nearly 97% of TD. The thermal conductivity has a positive correlation with relative density, as shown in Fig. 2. It is obvious to understand that as three-dimensional defects, pores reduce the cross-sectional area in all directions of the samples, increasing the equivalent thermal resistance and impeding the conduction of phonons and electrons. Therefore, it is necessary to get higher density for obtaining high thermal conductivity of as-built samples. If the linear fit is inferred to be of 100% full density, the

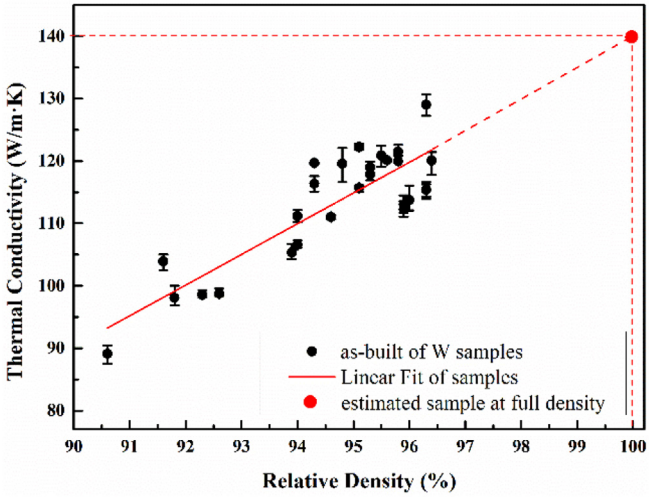

Fig. 2. Thermal conductivity plotted versus the relative density of as-built samples. The linear fit is extrapolated to estimate the theoretical thermal conductivity at full density.

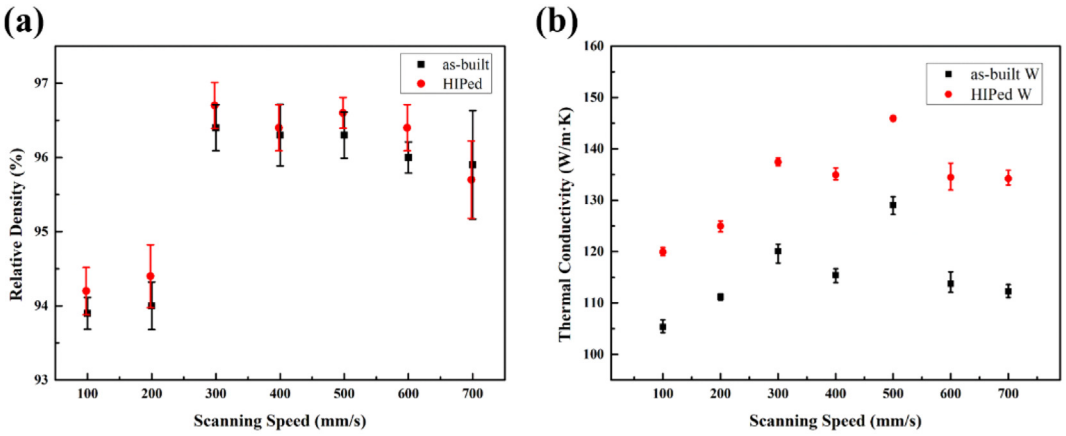

Fig. 3. (a) Variations in relative density with LPBF scanning speed of the as-built and post-HIPed samples with 100 μm hatch distance. (b) Thermal conductivity plotted versus scanning speed when 100 μm hatch distance is used, showing improved thermal conductivity at v = 300–500 mm/s before and after HIP.

theoretically non-porous AM tungsten sample with a thermal conductivity of 140 W/ (m· K) could be obtained, but still differs by > 20 W/ (m· K) compared with theoretical pure tungsten. The difference indicates a significant role of micro-cracks, grain boundaries, and dislocations in addition to pores. Distribution of micro-cracks could have a small effect on density of samples, but a complicated effect on thermal conductivity.

As shown in Fig. 3a, when a scanning speed from 100 mm/s to 700 mm/s was used with 100 μm hatch distance, the relative density of the as-built and HIPed samples appears similar. The final volumetric energy density (E) of samples processed under different scanning speed is shown in Table 1. The volumetric energy density for the experiments carried out in the present study was calculated based on Eq. (2).

$$E = \frac{P}{h \times v \times t} \tag{2}$$

Where P is laser power, h is hatch distance, v is scanning speed and t is powder layer thickness. By taking into consideration of the finding made in Ref. [24] and the evolution of void size and shape by adjusting laser parameters, it is observed that a moderate scanning speed could minimize porosity when other laser parameters are constant. Interestingly, the density of the post-HIPed samples barely changes in comparison with that of the as-built samples, implying that as-built samples may contain open porosity. Even so, thermal conductivity is still significantly improved by nearly 20 $W{\cdot}m^{-1}{\cdot}K^{-1}$ after HIP treatment, as shown in Fig. 3b. The mean thermal conductivity of HIPed samples (133 $W{\cdot}m^{-1}{\cdot}K^{-1}$) is 16% higher than that of the as-built samples (115 $W{\cdot}m^{-1}{\cdot}K^{-1}$), with a maximum value of 146 $W{\cdot}m^{-1}{\cdot}K^{-1}$ after HIP treatment. Therefore, the evolution of cracks and microstructure under HIP process should be considered. Besides, some observations indicate that high density does not necessarily result in high thermal conductivity. To interpret this fact the uneven distribution of internal voids, cracks, and other microstructural defects needs to be considered.

Table 1
Summary of the W samples prepared for post-HIP treatment.

Laser power (W)	Layer thickness (μm)	Hatch spacing (μm)	Scan speed (mm/s)	Volumetric energy density (J/mm^3)
400	30	100	100	1333.3
400	30	100	200	666.7
400	30	100	300	444.4
400	30	100	400	333.3
400	30	100	500	266.7
400	30	100	600	222.2
400	30	100	700	190.5

3.2. Effect of post-HIP treatment on crack morphology and microstructure of LPBFed tungsten

The morphology of the surface cracks perpendicular to BD has a significant impact on thermal conductivity along BD. Fig. 4 shows the cracks' morphology and their distributions on the top surface before and after HIP treatment. From the top view of the as-built sample, as seen from Fig. 4b, longitudinal and transverse cracks along the molten tracks formed crack networks. Sharp crack tips can be clearly seen as indicated by red circles in Fig. 4c. Extensive intergranular-cracks clearly viewed around the molten tracks in the as-built samples are the result of thermal residual stresses exceeding the grain boundary fracture strength during the LPBF process. As the main defect type, micro-cracks would hinder the mobility of electrons and phonons, therefore reducing the thermal conductivity of the sample.

In contrast, the amount of micro-cracks in post-HIPed samples was obviously decreased, as seen in Fig. 4e. Passivated micro-cracks were found along the bonding line as indicated in red circles in Fig. 4f. After post-HIP treatment, the typical LPBF molten tracks have almost disappeared, and the grain morphology is similar to that of annealed tungsten [25]. During HIP treatment, micro-cracks were first closed by high temperature creep, then bonded together mechanically, and finally homogenized between metal layers [26]. In this situation, as pure tungsten samples are subjected to high temperature and high pressure simultaneously, cracks that were not connected to the outer surface of the parts were passivated and mechanically healed. Traces of the retained pristine molten tracks are marked with white curves in Fig. 4e and accompany cracks that were passivated and pressed into micro-voids with inner pressure equaling external pressure (180 MPa). Therefore, micro cracks could be almost healed by diffusion bonding during HIP processing, then transformed into micro-voids. In fact, similar studies have reported healed crack traces with discrete micro voids formed after HIP treatment [27,28]. In addition, as seen from Fig. 4d, there is one grain across the cracks marked in a red square frame, confirming that the grain growth across healed cracks happened. Therefore, micro-cracks can be eliminated by the bridging of metallic interfaces next to cracks on the XY plane, which is also beneficial to the improvement of thermal conductivity along BD.

Indeed, there is only one thermal conductivity parameter in bcc pure tungsten because thermal conductivity is a second order tensor. Different crystallographic orientations do not make an impact on thermal conductivity of tungsten. Only crystallographic defects, such as vacancies, grain boundaries and dislocations, are considered as main factors that affect the thermal conductivity of tungsten. EBSD maps were characterized to evaluate microstructure evolutions and determine the grain structure as shown in Fig. 4a and d. Grain growth in

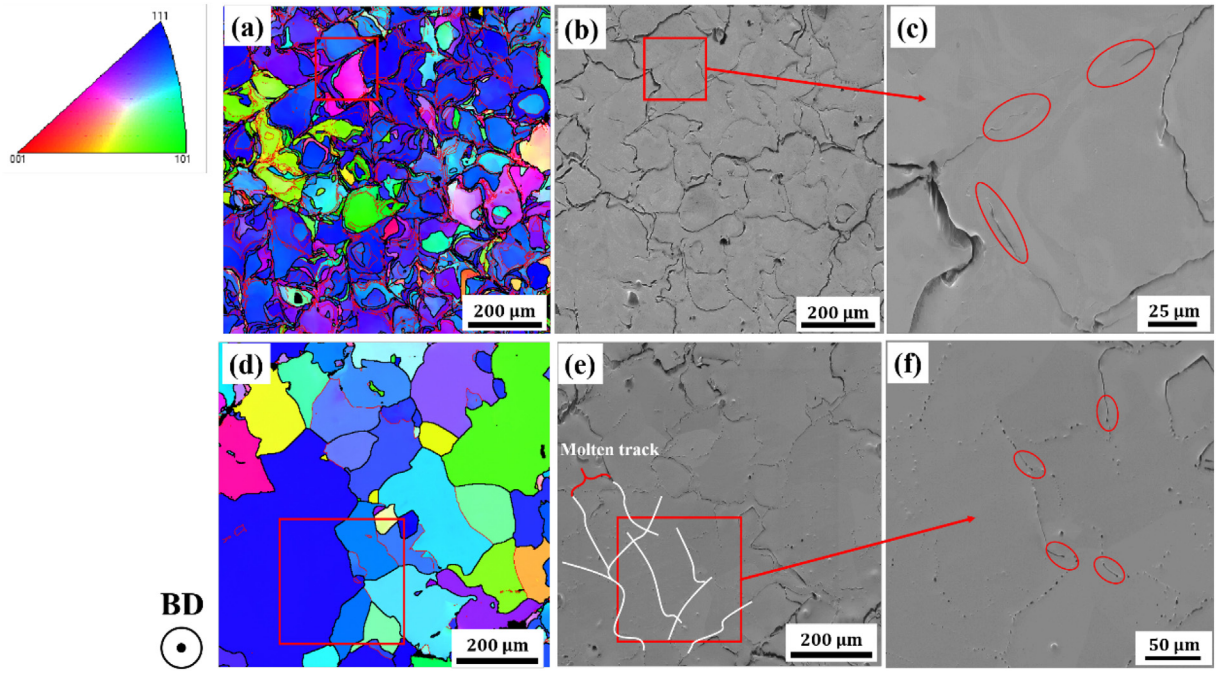

Fig. 4. The microstructure and crack distribution in as-built and post-HIPed samples from the top view: (a) IPF mapping and (b, c) corresponding SEM image of the as-built sample, (d) IPF mapping and (e, f) corresponding SEM image of the post-HIPed sample. Molten tracks are marked by white curves while crack tips and passivated cracks are indicated by red circles. The red lines in (a, d) represent subgrain boundaries (misorientation < 15°) whereas black lines represent grain boundaries (misorientation > 15°). (For interpretation of the references to colour in this figure legend, the reader is referred to the web version of this article.)

the post-HIPed sample can be clearly observed in the IPF map of the top face. After post-HIP treatment, the grains grew to over 300 μm in size. Quantitatively, the grains with size larger than 200 μm accounted for 60% of the total area after post-HIP, whereas this figure was < 10% in as-built samples.

A possible mechanism for this phenomenon could be that the applied HIPing temperature of 1800 °C is high enough to facilitate atomic diffusion thus to accelerate the grain boundary motion. Rapid solidification and high temperature gradients in LBPF process can induce residual thermal stress and uneven deformation. Dispersed uneven deformation energy storage at high temperature and pressure can bring about high-energy circular-arc shaped grains tending to move towards the distortion area, promoting boundary migration to reverse the center of curvature, resulting in straight and flat boundaries after post-HIP. In addition, the reduction in the number of subgrain boundaries also indicates that the recovery or recrystallization process may take place during post-HIP. Smaller grains increase the chance of phonon and phonon scattering at grain boundaries [29,30]. After HIP treatment, grain size increased, less grain boundaries acted as two-dimensional defects, therefore weakening the phonon and electron scattering, which is favorable to obtain higher thermal conductivity.

In order to illustrate residual plastic deformation after post-HIP treatment, kernel average misorientation (KAM) mapping was conducted, as shown in Fig. 5a and c, where the green reflects the cluster of dislocations. In as-built tungsten, the deformation was mainly concentrated around the voids, crack tips as well as subgrain boundaries. While in HIPed tungsten, the local misorientation difference in a single grain almost disappeared, which demonstrates the reduction of dislocation densities. The quantitative statistics in Fig. 5b and d also reveal that the proportion of subgrain boundaries after post-HIP is significantly reduced from 0.585 to 0.224, and the area weighted grain size is distinctly increased from 84.33 μm to 224.71 μm.

The subgrain boundary can be explained by dislocation theory. Indeed, some classical defects found in grain structures, such as point defects and dislocations, provide more scattering circumstances and shorten the mean free path of phonons, decreasing the intrinsic thermal conductivity. Accumulation of the residual stress is also reflected by a large number of stacking dislocations during rapid solidification. The thermal conductivity of materials is strongly limited by the presence of dislocations when they exceed a certain density at room temperature where a logarithmic dependence is found [31]. Even if high stacking fault energy exists in dislocations that are difficult to move, they can be set in motion by climbing and gliding during the HIP environment. Subgrain merging and the disappearance of local misorientation occurs through dislocation interactions. The annihilation of dislocations can reduce phonon and electron scattering, improving the thermal conductivity of tungsten samples.

As a whole, the introduced HIP treatment promotes the grain growth and reduces dislocation density, as well as healing micro-cracks, thus enhancing the thermal conductivity of LPBFed tungsten. Further research in changing the laser parameters and optimizing HIP process parameters will be considered to obtain homogeneous microstructure and crack-free samples, which might have the potential to obtain theoretical thermal conductivity of tungsten using LPBF technique.

4. Conclusions

(1) Thermal conductivity is improved in as-built tungsten when a moderate scanning speed is used with other constant laser parameters (In this study, v = 300–500 mm/s, E = 444.4–266.7 J/mm^3). There is a positive correlation between thermal conductivity and sample density, indicating that density significantly affects the thermal conductivity of as-built tungsten. To get higher thermal conductivity, samples should be built with higher density.

(2) Post-LPBF treatment can improve thermal conductivity of pure tungsten to 146 $W \cdot m^{-1} \cdot K^{-1}$. The average value of the thermal conductivity after HIP was increased by 16%, which could not be attributed to the density increase. HIP treatment improves thermal conductivity of LPBFed tungsten samples by healing micro-cracks and reducing microstructural defects such as grain boundaries and subgrains.

(3) HIP treatment promotes grain growth, reduces dislocation density,

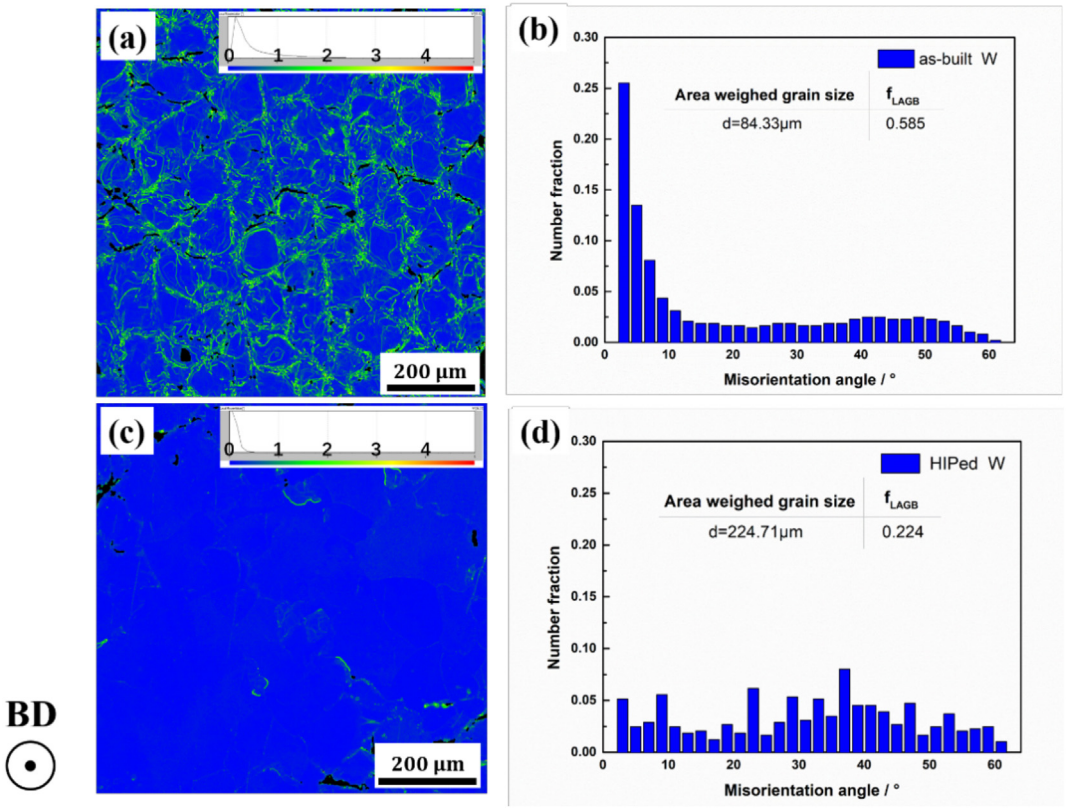

Fig. 5. KAM mapping of pure tungsten analyzed by EBSD perpendicular to BD of (a) as-built and (c) the post-HIPed samples. Diagrams illustrate variations between subgrain boundary fraction and misorientation angle of (b) the as-built and (d) the post-HIPed tungsten samples corresponding to KAM images of (a) and (c), respectively. Note that the KAM maps (a, c) were calculated from Fig. 4 (a) and (c), respectively, which demonstrate the local misorientation and dislocation densities in tungsten material.

and bridges micro-cracks, thereby increasing the intrinsic thermal conductivity of LPBFed tungsten. A combination of changing the laser parameters and optimizing HIP process parameters could be further explored to obtain uniform microstructures as well as virtually crack-free samples to obtain the theoretical thermal conductivity of tungsten.

Acknowledgements

The authors acknowledge the financial support of the National Magnetic Confinement Fusion Science Program of China [Grant number 2014GB117000]; and the National Natural Science Foundation of China [Grant number U1605243].

Conflict of interest: None.

References

[1] V. Philipps, Tungsten as material for plasma-facing components in fusion devices, J. Nucl. Mater. 415 (2011) S2–S9.
[2] D. Zhang, Q. Cai, J. Liu, Formation of nanocrystalline tungsten by selective laser melting of tungsten powder, Mater. Manuf. Process. 27 (2012) 1267–1270.
[3] S. Wurster, N. Baluc, M. Battabyal, T. Crosby, J. Du, C. García-Rosales, et al., Recent progress in R&D on tungsten alloys for divertor structural and plasma facing materials, J. Nucl. Mater. 442 (2013) (S181-S9).
[4] M. Fukuda, A. Hasegawa, S. Nogami, Thermal properties of pure tungsten and its alloys for fusion applications, Fusion Eng. Des. 132 (2018) 1–6.
[5] Y. Zhong, L.-E. Rännar, S. Wikman, A. Koptyug, L. Liu, D. Cui, et al., Additive manufacturing of ITER first wall panel parts by two approaches: selective laser melting and electron beam melting, Fusion Eng. Des. 116 (2017) 24–33.
[6] E.C. Santos, M. Shiomi, K. Osakada, T. Laoui, Rapid manufacturing of metal components by laser forming, Int J Mach Tool Manu 46 (2006) 1459–1468.
[7] M.T. Andani, N. Shayesteh Moghaddam, C. Haberland, D. Dean, M.J. Miller, M. Elahinia, Metals for bone implants. Part 1. Powder metallurgy and implant rendering, Acta Biomater. 10 (2014) 4058–4070.
[8] X. Zhang, Q. Yan, S. Lang, M. Xia, C. Ge, Texture evolution and basic thermal–mechanical properties of pure tungsten under various rolling reductions, J. Nucl. Mater. 468 (2016) 339–347.
[9] D.-Z. Wang, K.-L. Li, C.-F. Yu, J. Ma, W. Liu, Z.-J. Shen, Cracking behavior in additively manufactured pure tungsten, Acta Metall. Sin. (English Letters) 32 (2018) 127–135.
[10] X. Zhou, X. Liu, D. Zhang, Z. Shen, W. Liu, Balling phenomena in selective laser melted tungsten, J. Mater. Process. Technol. 222 (2015) 33–42.
[11] D. Wang, C. Yu, X. Zhou, J. Ma, W. Liu, Z. Shen, Dense pure tungsten fabricated by selective laser melting, Appl. Sci. 7 (2017).
[12] C. Tan, K. Zhou, W. Ma, B. Attard, P. Zhang, T. Kuang, Selective laser melting of high-performance pure tungsten: parameter design, densification behavior and mechanical properties, Sci. Technol. Adv. Mater. 19 (2018) 370–380.
[13] R.K. Enneti, R. Morgan, S.V. Atre, Effect of process parameters on the selective laser melting (SLM) of tungsten, Int. J. Refract. Met. Hard Mater. 71 (2018) 315–319.
[14] K. Kempen, B. Vrancken, S. Buls, L. Thijs, J. Van Humbeeck, J.-P. Kruth, Selective laser melting of crack-free high density M2 high speed steel parts by baseplate preheating, J. Manuf. Sci. Eng. 136 (2014).
[15] I. Yadroitsev, P. Krakhmalev, I. Yadroitsava, S. Johansson, I. Smurov, Energy input effect on morphology and microstructure of selective laser melting single track from metallic powder, J. Mater. Process. Technol. 213 (2013) 606–613.
[16] D. Wang, Z. Wang, K. Li, J. Ma, W. Liu, Z. Shen, Cracking in laser additively manufactured W: initiation mechanism and a suppression approach by alloying, Mater. Des. 162 (2019) 384–393.
[17] K. Li, D. Wang, L. Xing, Y. Wang, C. Yu, J. Chen, et al., Crack suppression in additively manufactured tungsten by introducing secondary-phase nanoparticles into the matrix, Int. J. Refract. Met. Hard Mater. 79 (2019) 158–163.
[18] G. Pintsuk, H. Kurishita, J. Linke, H. Arakawa, S. Matsuo, T. Sakamoto, et al., Thermal shock response of fine- and ultra-fine-grained tungsten-based materials, Phys. Scr. T145 (2011).
[19] S.E. Landwehr, G.E. Hilmas, W.G. Fahrenholtz, I.G. Talmy, S.G. DiPietro, Microstructure and mechanical characterization of ZrC–Mo cermets produced by hot isostatic pressing, Mater. Sci. Eng. A 497 (2008) 79–86.
[20] Z. Tang, O.N. Senkov, C.M. Parish, C. Zhang, F. Zhang, L.J. Santodonato, et al., Tensile ductility of an AlCoCrFeNi multi-phase high-entropy alloy through hot isostatic pressing (HIP) and homogenization, Mater. Sci. Eng. A 647 (2015) 229–240.
[21] B. Ruttert, M. Ramsperger, L. Mujica Roncery, I. Lopez-Galilea, C. Körner, W. Theisen, Impact of hot isostatic pressing on microstructures of CMSX-4 Ni-base superalloy fabricated by selective electron beam melting, Mater. Des. 110 (2016) 720–727.
[22] Z. Oksiuta, K. Perkowski, M. Osuchowski, M. Zalewska, M. Andrzejczuk,

Microstructure and thermal properties of mechanically alloyed W-1%TiC powder consolidated via two-step HIPping, Fusion Eng. Des. 126 (2018) 51–58.
[23] Y.K. Wang, S. Miao, Z.M. Xie, R. Liu, T. Zhang, Q.F. Fang, et al., Thermal stability and mechanical properties of HfC dispersion strengthened W alloys as plasma-facing components in fusion devices, J. Nucl. Mater. 492 (2017) 260–268.
[24] S. Wen, C. Wang, Y. Zhou, L. Duan, Q. Wei, S. Yang, et al., High-density tungsten fabricated by selective laser melting: densification, microstructure, mechanical and thermal performance, Opt. Laser Technol. 116 (2019) 128–138.
[25] C. Ren, Z.Z. Fang, M. Koopman, B. Butler, J. Paramore, S. Middlemas, Methods for improving ductility of tungsten - a review, Int. J. Refract. Met. Hard Mater. 75 (2018) 170–183.
[26] X. Zhao, X. Lin, J. Chen, L. Xue, W. Huang, The effect of hot isostatic pressing on crack healing, microstructure, mechanical properties of Rene88DT superalloy prepared by laser solid forming, Mater. Sci. Eng. A 504 (2009) 129–134.
[27] M.N. Gussev, N. Sridharan, Z. Thompson, K.A. Terrani, S.S. Babu, Influence of hot isostatic pressing on the performance of aluminum alloy fabricated by ultrasonic additive manufacturing, Scr. Mater. 145 (2018) 33–36.
[28] P. Mellin, H. Magnusson, P. Harlin, S. Wikman, J. Olsén, Z.J. Shen, et al., Bonding EBM-built blocks of 316L Steel, using hot isostatic pressing, in: D.P. Blanchard (Ed.), Euro PM2017 Congress & Exhibition, 2017 Milan, Italy.
[29] H. Dong, B. Wen, R. Melnik, Relative importance of grain boundaries and size effects in thermal conductivity of nanocrystalline materials, Sci. Rep. 4 (2014).
[30] A. Sood, R. Cheaito, T. Bai, H. Kwon, Y. Wang, C. Li, et al., Direct visualization of thermal conductivity suppression due to enhanced phonon scattering near individual grain boundaries, Nano Lett. 18 (2018) 3466–3472.
[31] C. Mion, J.F. Muth, E.A. Preble, D. Hanser, Thermal conductivity, dislocation density and GaN device design, Superlattice. Microst. 40 (2006) 338–342.